This is the author pre-publication version. This paper does not include the changes arising from the revision, formatting and publishing process. The final paper that should be used for referencing is:

A. Gardi, R. Sabatini and S. Ramasamy, "Stand-off Measurement of Industrial Air Pollutant Emissions from Unmanned Aircraft." Proceedings of IEEE International Conference on Unmanned Aircraft Systems (ICUAS 2016). Arlington, VA (USA), June 2016. Print ISBN: 978-1-4673-9333-1

# Stand-off Measurement of Industrial Air Pollutant Emissions from Unmanned Aircraft

Alessandro Gardi, Roberto Sabatini and Subramanian Ramasamy

*RMIT University, Melbourne, Australia*

***Abstract*– This paper investigates the stand-off measurement of atmospheric pollutant concentrations and air quality parameters around industrial complexes. The theoretical investigation considers a robust, accurate and inexpensive measurement system based on tuneable Light Detection and Ranging (LIDAR), calibrated reflectors and imaging systems. The equipment is deployed in two non-collocated components. The source component is installed on board an unmanned aircraft. The sensor component is constituted by a reflector calibrated for reflectance, a rail-mounted infrared camera calibrated for radiance and highly wavelength-selective optics. The system is conceived to perform Differential Absorption LIDAR (DIAL) measurements of selected molecular pollutants and a model-based estimation of aerosol pollutant concentrations by means of suitably developed inversion algorithm. The relevant opportunities and challenges, and the viability of the system in the intended operational environments are discussed. Numerical simulation results show promising performances in term of estimated error budget even in degraded meteorological conditions, which are comparable to the more complex and relatively costly monostatic LIDAR techniques currently available.**

## I. INTRODUCTION

A number of metrological techniques have been developed and successfully utilised for atmospheric pollutant measurements. These techniques are classified based on whether they involve the in-situ sampling of emissions from specific processes or the remote sensing [1]. In most of the industrial and transport contexts, emissions are locally measured by air quality sampling stations and bench measurement systems based on in-situ extraction-sampling techniques involving optical spectroscopy, mass spectrometry or other chemical measurement principles. In-situ sampling devices are nevertheless limited as they can only produce point measurements and are not well suited to characterise the spatial distribution of pollutants and the peak locations. Furthermore, at increasing distances from the emission source, the accuracy of the real-time emissions dispersion mapping is negatively affected by the advection/diffusion processes. Technological advances in tuneable laser sources allowed them to progressively achieve lower Size, Weight and Power (SWaP) characteristics, allowing for different laser sounding systems to be deployed on aircraft, satellites or other aerial/surface vehicles. Differential Absorption LIDAR (DIAL) remote sensing is based on volume scattering measurements and has been deployed on a number of ground-based, aerial and satellite platforms for atmospheric sounding [2-11]. Remote sensing by monostatic DIAL systems based on coherent detection of back-scattered radiation allow to flexibly scan extended geographic areas and accurately determine the spatial distribution of pollutants but are typically very expensive both in terms of equipment and operation, especially when longer ranges are considered, and also frequently not available when and where required. This severely limits their viability when the measurement of specific industrial processes or individual pollutant emission sources is considered. Given the growing public awareness and political pressure with respect to air quality and climate change, it is expected that both the environmental protection policies and monitoring activities will be further extended. The viability of future emissions trading and taxation schemes will crucially depend on trustworthy monitoring by organisations, for issuing permits and calculating charges. More accurate and verifiable pollution measurement techniques are needed to ensure transparency in regulation, as well as fair and accurate pricing under these schemes. In order to address the public concerns and simultaneously empower the scientific research activities, it is crucial to accurately determine the pollutant concentrations at the required scale and resolutions around the polluting sources employing relatively inexpensive and technologically mature equipment. By design, novel measurement techniques for atmospheric pollutants based on bistatic LIDAR can overcome limitations of both in-situ extraction sampling and remote sensing systems currently available, potentially meeting the requirements set by the air transport industry as well as various other industrial sectors. In particular, the full potential of the proposed bistatic LIDAR measurement system could be explored when its functional integration in the next generation of Air Traffic Management (ATM) systems is considered, as the continuous monitoring of pollutant emissions could be exploited to drive the reconfiguration of arrival/departure routes and airspace structure in real-time [12, 13].

This is the author pre-publication version. This paper does not include the changes arising from the revision, formatting and publishing process. The final paper that should be used for referencing is:

A. Gardi, R. Sabatini and S. Ramasamy, "Stand-off Measurement of Industrial Air Pollutant Emissions from Unmanned Aircraft." Proceedings of IEEE International Conference on Unmanned Aircraft Systems (ICUAS 2016). Arlington, VA (USA), June 2016. Print ISBN: 978-1-4673-9333-1

## II. Conceptual Design

A stand-off measurement system based on bistatic LIDAR techniques was conceptually investigated in [14-16], based on previous research [6, 17-19]. The principle of operation of the aerial monitoring by an Unmanned Aircraft (UA) employing bistatic LIDAR measurement techniques is depicted in Fig. 1. Both molecular and aerosol concentrations in the atmosphere introduce absorption and scattering phenomena that affect the laser beam propagation. While molecular absorption and scattering are highly wavelength-selective and enable DIAL measurements, aerosols do not manifest measurable wavelength-selective absorption and scattering within the limited tuneability spectrum of the LIDAR emitter, and therefore require suitably developed knowledge-based inversion algorithms. The receiver is composed by a calibrated target surface of high and diffused reflectance exhibiting Lambertian behaviour and a NIR camera with receiver (RX) optics mounted on a rail. A Bidirectional Reflectance Distribution Function (BRDF) is derived for the calibrated target surface. Highly selective filters are used as part of the RX optics on the NIR camera to detect the laser spot energy on the target and to generate a Pixel Intensity Matrix (PIM) in a high resolution greyscale format. As conceptually represented in Fig. 2, the proposed stand-off measurement system consists of two non-collocated components.

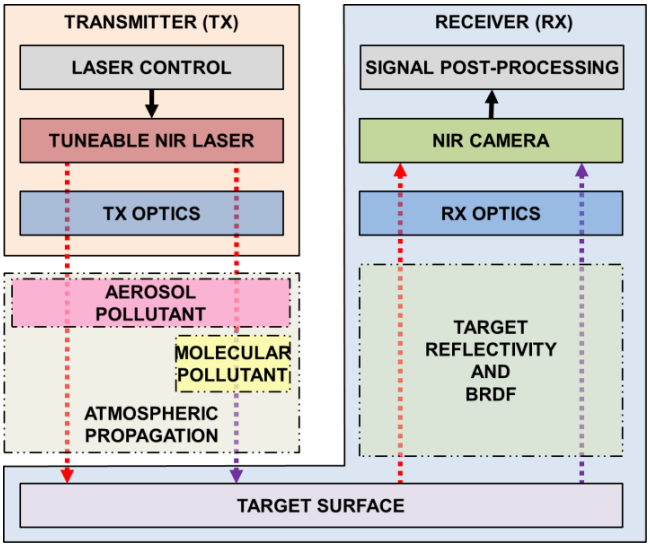


Fig. 1. Functional block diagram of the bistatic LIDAR measurement system.

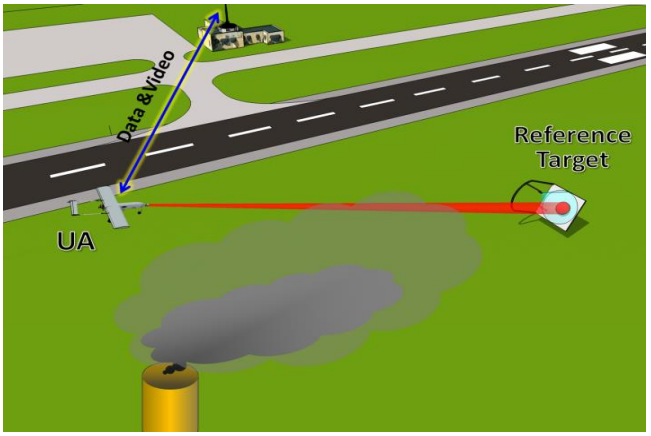


Fig. 2. Bistatic LIDAR system, not to scale.

A LIDAR emitter is installed on a UA. The sensor component consists of a target surface featuring high and diffused reflectance and exhibiting Lambertian behaviour, such as Spectralon™, and a visible/infrared camera mounted on a rail. The UA platform flies pre-determined trajectories based on the required space and time frames of the measurement.In [14] we presented the key features of the measuring system, discussed the rationale supporting its development and introduced one measurement technique. An in situ calibration technique was also introduced, employing a second ground-based LIDAR emitter and electro-optics photo-detectors. This paper reviews and updates our theoretical developments with an identification of operational and technical requirements for a first experimental prototype system to be employed on a suitable UA platform. The measurement of molecular pollutant species is based on the DIAL technique. The laser source emits beams at two predefined wavelengths. The first wavelength ($\lambda_{ON}$) is selected in correspondence of a major vibrational band of the targeted pollutant molecule (on-absorption line), clear from the transition/vibration spectrum of other atmospheric components. The second wavelength ($\lambda_{OFF}$) is selected in proximity of the first, but outside the vibrational band (off-absorption line) of the targeted pollutant species, so that the difference in cross-sections, $\Delta\psi \triangleq \psi(\lambda_{ON}) - \psi(\lambda_{OFF})$ is maximised. A number of databases and atmospheric Radiative Transfer Model (RTM) codes are available and allow an accurate estimation of the propagation spectrum for identifying the optimal combination of DIAL wavelengths based on the mentioned criteria.

This is the author pre-publication version. This paper does not include the changes arising from the revision, formatting and publishing process. The final paper that should be used for referencing is:

A. Gardi, R. Sabatini and S. Ramasamy, "Stand-off Measurement of Industrial Air Pollutant Emissions from Unmanned Aircraft." Proceedings of IEEE International Conference on Unmanned Aircraft Systems (ICUAS 2016). Arlington, VA (USA), June 2016. Print ISBN: 978-1-4673-9333-1

## III. Reference UA Platform

The reference platform for future system development stages is the AEROSONDE UA, which is a small autonomous aircraft used in weather-reconnaissance and remote-sensing missions. The AEROSONDE UA is capable of extended surveillance and reconnaissance over land and sea in a variety of environmental conditions, delivering real-time information persistently and reliably. The AEROSONDE UA offers an endurance of more than 26 hours (with minimal payload). With a full electro-optic/infrared payload, the AEROSONDE UA can still achieve endurances in excess of 10 hours. This impressive endurance, as well as the aircraft's payload flexibility, modularity and affordability, make it an ideal choice for remote data collection and reconnaissance missions for military, civil and scientific entities. The aircraft employs a catapult system to take off from small, remote clearings and ships, and can also launch from the roof of a fast-moving ground vehicle. The AEROSONDE Mark 4.7 specifications are provided below:

**Airframe**

- Wing span: 3.6 m;
- Maximum gross take-off weight: 17.5 kg (J-type engine) 25 kg (K-twin engine);
- Cruise speed: 50~60 knots;
- Dash speed: 62~80 knots at sea level;
- Ceiling: 15,000 ft (4,500) m density altitude;
- Endurance: 10 hours or more (including payloads);
- Lights: Visible navigation lights and IR anti-collision lights;

**Payload Capacity**

- 12 in x 9.5 in x 9.5 in (≈ 1,000 $in^3$);
- Weight 7.5 ~10 pounds;
- 75-190 watts available.

**Avionics**

- Primary data link: 300 MHz, or UHF (Mil band);
- Secondary data link: 300/1,300 MHz (Mil band);
- BLOS data link: C-band (4-8 GHz), $K_a$ band (26.5–40 GHz) and Ku band (12–18 GHz);
- Transponder: Mode 3 Identification Friend or Foe (IFF) and Mode S;
- Navigation Sensors/ Systems: Global Navigation Satellite System (GNSS), Inertial Measurement Unit (IMU), Vision Based Navigation (VBN) sensor and Aircraft Dynamics Model (ADM) augmentation;
- Back-up battery (20 W-hr);
- Three-axis magnetometer;
- Optional laser altimeter
- Avionics power: 18 volts direct current, or VDC;
- Payload power: 15 VDC.

**Power Plant**

- J-type engine: four-stroke, 24 $cm^3$ Electronic Fuel Injection (EFI);
- K-twin engine upgrade: dual cylinder, four-stroke, EFI;
- Fuel: 93 octanes (premium) or 100 octanes low-lead aviation gas (AvGas).

**Launch and recovery**

- Auto launch;
- Auto belly or net recovery.

## IV. Pollutant Dispersion Model

A knowledge-based estimation of the pollutant dispersion plume is implemented to assist in defining the best stand-off sensing patterns and extrapolate the measurement data to reconstruct the full plume profile from a limited number of soundings. This approach can crucially enhance system safety and provide pollutant concentration estimates in real-time over a wide area without necessitating multiple UA. A fixed point emission source is assumed, and the Cartesian reference frame is defined so that X axis is orientated along the free stream flow velocity. By adopting Fick's law of diffusion, assuming statistical turbulence models with suitable assumptions, the concentration of the pollutant $\Pi$ can be expressed as:

$$[\Pi] = \frac{\dot{m}}{2\pi v \sigma_y \sigma_z} \cdot \left\{ \begin{array}{l} \exp\left(-\frac{y^2}{2\kappa_y^2} - \frac{(z-h)^2}{2\kappa_z^2}\right) + \\ + \exp\left(-\frac{y^2}{2\kappa_y^2} - \frac{(z+h)^2}{2\kappa_z^2}\right) \end{array} \right\} \quad (1)$$

Where $\dot{m}$ represent the pollutant mass flow, $\kappa$ are dispersion parameters, which depend on position, v represent the free stream velocity, h is the height of the point emission source from the ground. The dispersion parameters depend on the distance from the source.

This is the author pre-publication version. This paper does not include the changes arising from the revision, formatting and publishing process. The final paper that should be used for referencing is:

A. Gardi, R. Sabatini and S. Ramasamy, "Stand-off Measurement of Industrial Air Pollutant Emissions from Unmanned Aircraft." Proceedings of IEEE International Conference on Unmanned Aircraft Systems (ICUAS 2016). Arlington, VA (USA), June 2016. Print ISBN: 978-1-4673-9333-1

The Pasquill-Gifford model is most commonly adopted to empirically express the dependence on the distance and on local environmental conditions. Table 1 details the classification of plume stability based on environmental conditions, while Table 2 provides the relationships for $\kappa_z$ . Figure 3 represents the dispersion plume parameters. A conceptual representation of one possible scanning pattern that can be executed by the UA to map the pollutant concentration is given in Figure 4.

TABLE I. PASQUILL STABILITY CLASSIFICATION BASED ON ENVIRONMENTAL CONDITIONS

| **Freestream velocity** | **Daytime incoming solar radiation** | | | **Night time cloud cover** | |
|---|---|---|---|---|---|
| m/s | Strong | Moderate | Slight | > 50% | < 50% |
| < 2 | A | A – B | B | E | F |
| 2 – 3 | A – B | B | C | E | F |
| 3 – 5 | B | B – C | C | D | E |
| 5 – 6 | C | C – D | D | D | D |
| > 6 | C | D | D | D | D |

TABLE II. EMPIRICAL RELATIONSHIPS

| Stability class | $x\ [m]$ | $\sigma_z\ [m]$ |
|---|---|---|
| A | 100~300<br>300~3000 | $\sigma_z = 0.287\ x^{0.88}$<br>$\log_{10}\sigma_z = -1.67 + 0.902\ \log_{10} x + 0.181\ (\log_{10} x)^2$ |
| B | 100~500<br>500~2E+4 | $\sigma_z = 0.135\ x^{0.95}$<br>$\log_{10}\sigma_z = -1.25 + 1.09\ \log_{10} x + 0.0018\ (\log_{10} x)^2$ |
| C | 100~$10^5$ | $\sigma_z = 0.112\ x^{0.91}$ |
| D | 100~500<br>500~$10^5$ | $\sigma_z = 0.093\ x^{0.85}$<br>$\log_{10}\sigma_z = -1.22 + 1.08\ \log_{10} x - 0.061\ (\log_{10} x)^2$ |
| E | 100~500<br>500~$10^5$ | $\sigma_z = 0.082\ x^{0.82}$<br>$\log_{10}\sigma_z = -1.19 + 1.04\ \log_{10} x - 0.070\ (\log_{10} x)^2$ |
| F | 100~500<br>500~$10^5$ | $\sigma_z = 0.057\ x^{0.8}$<br>$\log_{10}\sigma_z = -0.91 + 1.37\ \log_{10} x - 0.119\ (\log_{10} x)^2$ |

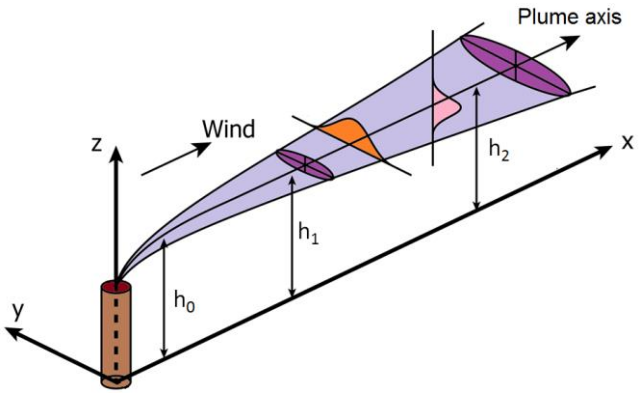


Fig. 3. Dispersion plume parameters.

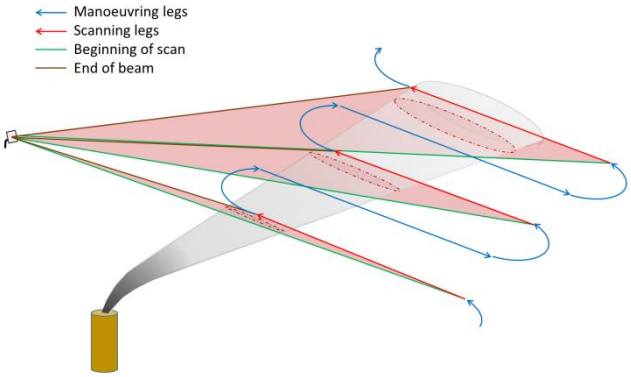


Fig. 4. Possible scanning pattern (not to scale).

## V. ATMOSPHERIC LASER BEAM PROPAGATION

The propagation of laser radiation in atmosphere is affected by a number of linear and nonlinear effects. In [15] we described the following expression for the peak irradiance $I_P$, accounting for absorption, scattering, diffraction, jitter, atmospheric turbulence and thermal blooming effects assuming a Gaussian profile of the laser beam at the source and an average focused irradiance [19, 20]:

$$I_P(z,\lambda) = \frac{b(z)\,\tau(z,\lambda)\,P(\lambda)}{\pi\left(a_d^2(z,\lambda) + a_j^2(z) + a_t^2(z,\lambda)\right)} \quad (2)$$

where $z$ is the linear coordinate along the beam, $\lambda$ is the wavelength, $P(\lambda)$ is the transmitted laser power, $b$ is the blooming factor, $\tau(z,\lambda)$ is the transmittance coefficient, which accounts for absorption and scattering associated with all molecular and aerosol species present in the path. The 1/e beam radiuses associated with diffraction, $a_d(z,\lambda)$, beam jitter, $a_j(z)$, and turbulence, $a_t(z,\lambda)$, can be calculated as [18, 20]:

$$a_d(z,\lambda) = \frac{Qz\lambda}{2\pi a_0} \quad (3)$$

$$a_j^2(z) = 2\langle\Theta_x^2\rangle\, z^2 \quad (4)$$

This is the author pre-publication version. This paper does not include the changes arising from the revision, formatting and publishing process. The final paper that should be used for referencing is:

A. Gardi, R. Sabatini and S. Ramasamy, "Stand-off Measurement of Industrial Air Pollutant Emissions from Unmanned Aircraft." Proceedings of IEEE International Conference on Unmanned Aircraft Systems (ICUAS 2016). Arlington, VA (USA), June 2016. Print ISBN: 978-1-4673-9333-1

$$a_t(z,\lambda) = \frac{2\,C_N^{6/5} z^{8/5}}{\lambda^{1/5}} \tag{5}$$

where $Q$ is the beam quality factor, $a_o$ is the beam *1/e* radius, $\langle \Theta_x^2 \rangle$ is the variance of the single axis jitter angle that is assumed to be equal to $\langle \Theta_y^2 \rangle$, and $C_N^2$ is the refractive index structure constant. An empirical model for the blooming factor $b(z)$, which is the ratio of the bloomed $I_B$ to unbloomed $I_{UB}$ peak irradiance, is:

$$b(z) = \frac{I_B}{I_{UB}} = \frac{1}{1 + 0.0625\, N^2(z)} \tag{6}$$

$N$ is the thermal distortion parameter, calculated as:

$$N(z) = \frac{-n_T\, \alpha_m\, P\, z^2}{\pi\, d_0\, v_0\, c_P\, a_0^3} \cdot \left[ \frac{2}{z^2} \int_0^R \frac{a_0}{a(z')}\, dz' \int_0^{z'} \frac{a_0^2\, v_0\, \tau''}{a}\, dz'' \right] \tag{7}$$

where $v_o$ is the uniform wind velocity in the weak attenuation limit ($\gamma z << 1$), $n_T$, $d_o$, and $c_p$ are, respectively, the coefficients of index change with respect to temperature, density, and specific heat at constant pressure. The transmittance coefficient $\tau$ depends on the integral effect of absorption and scattering phenomena, both for molecular and aerosol species, on the entire beam length. The expression of Beer's law highlighting such dependences can therefore be written as:

$$\tau(z,\lambda) = e^{-\int_0^z \gamma(z,\lambda)\, dz} =$$

$$= e^{-\int_0^z [\alpha_m(z,\lambda) + \alpha_a(z,\lambda) + \beta_m(z,\lambda) + \beta_a(z,\lambda)]\, dz} \tag{8}$$

where $\alpha$ are the absorption coefficients and $\beta$ are the scattering coefficients, the subscripts $m$ and $a$ refer respectively to molecular and aerosol contributions. When referring to the integral absorption and scattering due to specific molecular species, it is more appropriate to express the transmittance with the following model:

$$\tau(z,\lambda) = e^{-\int_0^z \gamma(z,\lambda)\, dz} = e^{-\int_0^z \sum_i [\psi_i(\lambda) \cdot n_i(z)]\, dz} \tag{9}$$

where:

$\psi_i(\lambda)$ = cross-section of the i$^{th}$ species

$n_i$ = molecular volume density of the i$^{th}$ species

From Eq. 9, the fraction between the measured incident laser energy associated with the on-absorption line of pollutant species $P$ and the one associated with the off-absorption line, $R_{ON/OFF}$, can be expressed as [14]:

$$R_{\frac{ON}{OFF}} = \frac{E(\lambda_{ON})}{E(\lambda_{OFF})} = \frac{\tau_{ON}}{\tau_{OFF}} =$$

$$= e^{-[\psi_P(\lambda_{ON}) - \psi_P(\lambda_{OFF})] \int_0^D n_P(r)\, dr} \tag{10}$$

where $D$ is the total beam length. The total pollutant column density $N_P$, which is the integral of the molecular volume density on the entire beam, is therefore:

$$N_P = \int_0^D n_P(r)\, dr = \frac{-\ln(R_{ON/OFF})}{\Delta\psi} \tag{11}$$

The average molecular volume concentration of the pollutant on the path, $\tilde{n}_P$, is therefore:

$$\tilde{n}_P = \frac{N_P}{D} = \frac{-\ln(R_{ON/OFF})}{D \cdot \Delta\psi} \tag{12}$$

As evident from Eq. 10 to 12, the bistatic DIAL measurement system neglects most of the parasite phenomena such as atmospheric visibility, particulate, rain and other precipitations, which would have elsewhere introduced a number of additional uncertainties in the system. The parasite effects, in fact, are assumed to equally affect the off-absorption and the on-absorption transmittances.

## VI. Particle Retrieval

The retrieval of aerosol concentrations was originally examined in [6]. As per eq. 8, both molecular and aerosol concentrations in the transmission medium (i.e. the atmosphere) introduce absorption and scattering phenomena that affect the laser beam propagation. Therefore, the atmospheric transmittance measurement data accumulated in a certain time period using passive imaging systems enable the retrieval of aerosol concentrations as well. The difficulty in developing inversion algorithms lies in the fact that the input optical data are related to the investigated microphysical parameters through nonlinear integral equations of the first kind (Fredholm equations), which cannot be solved analytically. The generalised form of the Fredholm equation for atmospheric data retrieval is:

$$\alpha(\lambda), \beta(\lambda) = \int K_{\alpha,\beta}(r,n,k,\lambda) \cdot D(r) dr \tag{13}$$

where $\alpha(\lambda)$, and $\beta(\lambda)$ represent the optical data, $K_{\alpha,\beta}$ is the atmospheric kernel function (containing information on particle size, refractive index etc.) and $D(r)$ is the particle size distribution. The numerical solution of these equations leads to the so called ill-posed inverse problem. Such problems are characterised by a strong sensitivity of the solution space toward uncertainties of the input data, the non-uniqueness of the solution space, and the incompleteness of the solution space. In fact, the solution space may still be correct in a mathematical sense, but might not necessarily reflect the physical conditions. As the problem cannot be entirely defined by the measurements, a priori knowledge of the state vector is required in order to determine the most probable solution, with a probabilistic Bayesian approach. Let $\boldsymbol{y}$ be the measurement vector containing the measured radiances, and $\boldsymbol{x}$ be the concentration of a given constituent, then the general remote sensing equation can be written as follows [21]:

$$\boldsymbol{y} = f(\boldsymbol{x}, \boldsymbol{b}) + \boldsymbol{\epsilon} \tag{14}$$

where $f$ represents the forward transfer function, $\boldsymbol{b}$ the other parameters affecting the measurement, and $\boldsymbol{\epsilon}$ the measurement noise.

This is the author pre-publication version. This paper does not include the changes arising from the revision, formatting and publishing process. The final paper that should be used for referencing is:

A. Gardi, R. Sabatini and S. Ramasamy, "Stand-off Measurement of Industrial Air Pollutant Emissions from Unmanned Aircraft." Proceedings of IEEE International Conference on Unmanned Aircraft Systems (ICUAS 2016). Arlington, VA (USA), June 2016. Print ISBN: 978-1-4673-9333-1

In the case of instruments measuring laser radiance, the vector $\boldsymbol{b}$ includes the target surface reflectance and radiance features (BRDF, reflectivity, emissivity and temperature), the variables describing the atmospheric state (vertical turbulence profile, temperature, water vapour and other atmospheric constituents, clouds, aerosols, etc.), and some characteristics of the measurement instruments (spectral response functions and resolution). The inverse problem consists in retrieving $\hat{\boldsymbol{x}}$, an estimate of the true state $\boldsymbol{x}$, from the measurement $\boldsymbol{y}$, and can be expressed as:

$$\hat{\boldsymbol{x}} = R(\boldsymbol{y}, \hat{\boldsymbol{b}}) = R\left(f(\boldsymbol{x}, \boldsymbol{b}) + \boldsymbol{\epsilon}, \hat{\boldsymbol{b}}\right) \quad (15)$$

where $\hat{\boldsymbol{b}}$ is an estimate of the non-retrieved parameters $\boldsymbol{b}$, and $R$ is the inverse transfer function. This a priori information consists of an a priori state vector $\boldsymbol{x_a}$ and its covariance matrix $\boldsymbol{S_a}$, which may be provided by model simulations. Therefore, the inverse problem can be rewritten as follows:

$$\hat{\boldsymbol{x}} = R(\boldsymbol{y}, \hat{\boldsymbol{b}}, \boldsymbol{x_a}) \quad (16)$$

Various inversion techniques were proposed. One of the most popular approaches is the inversion with regularisation, offering the advantage of reducing oscillations in the solution that are frequently experienced in data retrieved from electro-optical measurements [20, 22]. This approach consists in introducing constraints, such as derivative analysis (smoothness) of the particle size distribution functions, positive sign of the functions and maximum variations over time. The comprehensive inversion algorithm with regularisation is depicted in Fig. 5. Using appropriate kernel/base functions, this algorithm can deliver parameters such as effective (average) particle radius, particle size distribution, total surface-area concentration, total number/volume concentrations, real and imaginary parts of the refractive index, single scattering albedo, etc. The base functions are Gaussian fits of the existing particle concentration data and are used to reconstruct the investigated particle size distributions. The kernel functions describe the interaction of laser radiation with the atmosphere and contain information about the atmospheric transmittance, including scattering and absorption processes.

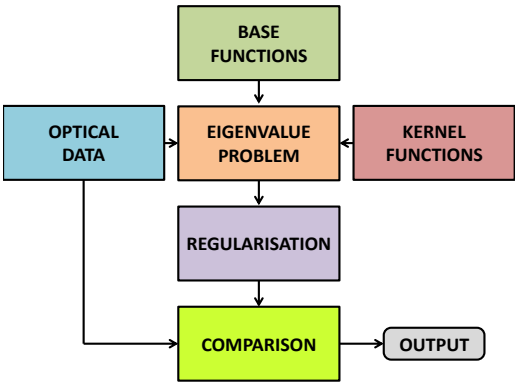


Fig. 5. Block diagram of the particle retrieval algorithm [6].

## VII. Model-Based Approach

Analytical expressions of the transmittances were developed for all the atmospheric windows in the infrared spectrum considering the parasite effects of atmospheric visibility, precipitation and fog [18]. By means of analytical inversion of the transmittance models, and thanks to an accurate sensing of local atmospheric conditions, it is also possible to determine the pollutant concentration without employing differential absorption measurements, by measuring the difference between the actually detected incident energy on the on-absorption line alone, and the model-based prediction for the off-absorption line. Although this technique simplifies the system architecture and potentially enable the adoption of less expensive non-tuneable laser emitters, the resulting error is heavily dependent on the quality and confidence of the measure of all parasite factors such as atmospheric visibility, temperature, pressure, humidity and precipitation. The theoretical model is based on comparison with the available extinction models for the $i^{th}$ atmospheric window [19]. By introducing the total condensed water along the laser beam path, $w$, the meteorological visibility, $V$, and the rainfall rate $R$ ,the empirically derived atmospheric transmittance values (off-absorption) for the 4$^{th}$ atmospheric window are summarised in Table 3 [19], where $k_{1,2\ldots6}$ are correction factors experimentally determined as in [18].

This is the author pre-publication version. This paper does not include the changes arising from the revision, formatting and publishing process. The final paper that should be used for referencing is:

A. Gardi, R. Sabatini and S. Ramasamy, "Stand-off Measurement of Industrial Air Pollutant Emissions from Unmanned Aircraft." Proceedings of IEEE International Conference on Unmanned Aircraft Systems (ICUAS 2016). Arlington, VA (USA), June 2016. Print ISBN: 978-1-4673-9333-1

TABLE III. EMPIRICAL EXPRESSIONS FOR THE ATMOSPHERIC OFF-ABSORPTION TRANSMITTANCE IN THE 4TH ATMOSPHERIC WINDOW [14].

| CONDITION | EMPIRICAL MODEL |
|---|---|
| $V \geq 6\ km, \quad w \geq 1.1\ mm$ | $\tau_{OFF}(z,w,V) \cong \mathrm{k}_1 \cdot 0.6432 \left(\frac{1.1}{w}\right)^{0.222} \cdot e^{-\frac{3.91}{V} z\, 0.3836^{-(0.0057V+1.025)}}$ |
| $V < 6\ km, \quad w \geq 1.1\ mm$ | $\tau_{OFF}(z,w,V) \cong \mathrm{k}_2 \cdot 0.6432 \left(\frac{1.1}{w}\right)^{0.222} \cdot e^{-\frac{3.91}{V} z\, 0.3836^{-0.585\sqrt[3]{V}}}$ |
| $V \geq 6\ km, \quad w < 1.1\ mm$ | $\tau_{OFF}(z,w,V) \cong \mathrm{k}_3 \cdot e^{-0.422\sqrt{w}-\frac{3.91}{V} z\, 0.3836^{-(0.0057V+1.025)}}$ |
| $V < 6\ km, \quad w < 1.1\ mm$ | $\tau_{OFF}(z,w,V) \cong \mathrm{k}_4 \cdot e^{-0.422\sqrt{w}-\frac{3.91}{V} z\, 0.3836^{-0.585\sqrt[3]{V}}}$ |
| rain and $w \geq 1.1\ mm$ | $\tau_{OFF}(z,w,R) \cong \mathrm{k}_5 \cdot e^{-0.422\sqrt{w}-0.365\, z\, R^{0.63}}$ |
| rain and $w < 1.1\ mm$ | $\tau_{OFF}(z,w,R) \cong \mathrm{k}_6 \cdot 0.6432 \left(\frac{1.1}{w}\right)^{0.222} \cdot e^{-0.365\, z\, R^{0.63}}$ |

The expressions of Table 3 are valid at mean sea level only. In order to extend the validity of the models, the dependency on altitude $h$ Above Mean Sea Level (AMSL) shall be introduced. A number of empirical relationships for the altitude correction have been experimentally determined for NIR lasers depending on the grazing angles [18]. Future research activities will be performed to further characterise the grazing angle dependency for the typical operational configurations of the UA bistatic DIAL measurement system.

## VIII. CALIBRATION

The photo-camera calibration is an experimental procedure that allows determination of the Integrated Radiance Response Function (AIRF) [18, 23]. A highly selective filter (i.e., response centred on the laser wavelength) is used in conjunction with the photo-camera to detect the laser spot energy on the target and to generate a Pixel Intensity Matrix (PIM) in a high resolution greyscale format. The calibration setup is shown in Fig. 6. The response of a single pixel in terms of Analogue Digital Unit (ADU) is:

$$ADU_{i,j} \propto \frac{A}{4 \cdot f_{\#}^2 + 1} \cdot g \cdot i_{time} \cdot \int_{\lambda_1}^{\lambda_2} (\tau_O \cdot \eta_D \cdot E_S)\, \mathrm{d}\lambda \quad (17)$$

where:

- $\lambda_{1,2}$ = limits of the photo-camera spectral band filter
- $\eta_D$ = detector quantum efficiency
- $E_S$ = spectral radiance
- $\tau_O$ = optics transmittance
- $A$ = pixel area
- $g$ = read-out electronics gain
- $f_{\#}$ = optics f-number
- $i_{time}$ = photo-camera integration time

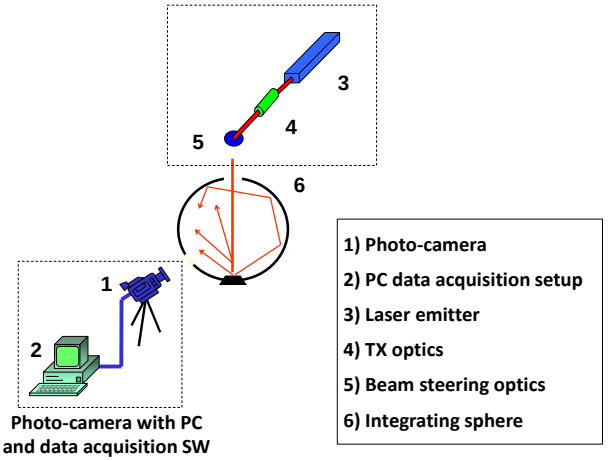


Fig. 6. Layout of the photo-camera calibration.

Therefore, the experimental parameters to be controlled during the calibration procedure are the integration time, the optics *f*-number and other settings of the photo-camera (e.g., the gain of the read-out electronics which may be selected by the operator). Fixing these parameters for a certain interval of integral radiance, it is possible to determine the AIRF of the camera by using an extended reference source.

This is the author pre-publication version. This paper does not include the changes arising from the revision, formatting and publishing process. The final paper that should be used for referencing is:

A. Gardi, R. Sabatini and S. Ramasamy, "Stand-off Measurement of Industrial Air Pollutant Emissions from Unmanned Aircraft." Proceedings of IEEE International Conference on Unmanned Aircraft Systems (ICUAS 2016). Arlington, VA (USA), June 2016. Print ISBN: 978-1-4673-9333-1

The function (calibration curve) so obtained is then used to determine the values of integral radiance for reconstructing the radiant intensity map of the target. Some mathematical models were developed and experimentally validated to calculate the optimal frame rate of the photo-camera [18]. In particular, photo-cameras are characterised by acquisition frequencies that typically are significantly different from the laser operating PRF. In the bistatic DIAL case, some additional consideration must be given to the alternated wavelengths of different pulses. A conceptual representation of the camera acquisition windows and dark zones in presence of laser pulses of alternating wavelength (different shades of red) is presented in Fig. 7. The parameters describing the train of pulses are the pulse duration ($\tau$), the pulse period ($T_P$) and the PRF ($f$). Similarly, the camera image acquisition process is defined by the frame period ($T_F$) and the camera acquisition time ($T_A$). Generally $T_A$ is inferior to $T_F$. The difference between $T_F$ and $T_A$ is the so called camera 'dark-time' ($T_{dark}$). Good synchronisation is extremely difficult even at low PRF and almost impossible as the PRF increases. Therefore a careful analysis is required in order to determine the optimal frame rate for the camera acquisition as a function of known laser pulse parameters. Since the camera frames are not synchronised with the laser pulses, considering the camera acquisition windows sequence as time base ($t_B$), the instant of arrival of the first laser pulse (reflected from the target) at the camera ($T_o$) can be treated as a random variable. Example results of a frame rate optimisation analysis, referred to laser emitters operating at $f$ = 10 Hz and $f$ = 40 kHz are summarised in Fig. 8, where $P_{err}$ is the error probability.

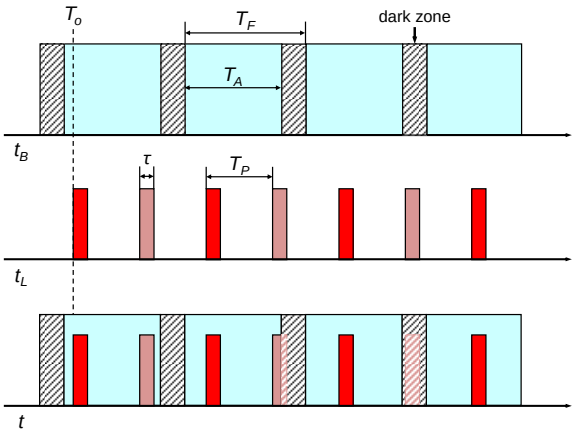


Fig. 7. Photo-camera acquisition sequence and laser pulses.

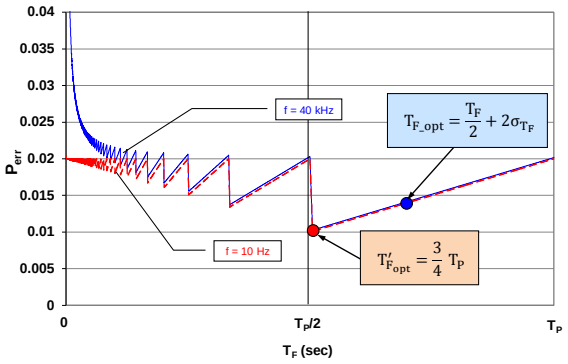


Fig. 8. NIR camera frame rate optimisation analysis.

## IX. In-Situ Calibration

The in-situ calibration technique of the bistatic LIDAR measurement system was described in [14]. In particular, an additional co-located NIR laser emitter and detector complex is installed on the ground at known distances from the first target surface and from an additional target surface, of equivalent specifications of the first, but without the NIR camera. The quality of the calibration is directly associated with the relative distance between the target surfaces, as evident from the following equations. As a reference, the assumed relative distances are, in particular, $\Delta d = d_2 - d_1 \geq 1\ km$. The anodic voltage at the receiver, $V$, can be expressed as [18]:

$$V = \mathrm{R_L} \cdot \mathrm{R_S} \cdot \mathrm{P}_R \tag{18}$$

where:

$\mathrm{R_L}$ = anodic load (Ω);

$\mathrm{R_S}$ = detector responsivity (A/W);

$\mathrm{P_R}$ = power reaching the detector (W);

By adopting two identical targets placed at different slant ranges, $d_1$ and $d_2$, at the same elevation above mean sea level (AMSL) at a similar bearing from the emitter/receiver, we can assume that the extinction coefficient on the off-absorption spectral line, $\gamma_{OFF}$, is constant between the two baselines. By detailing $P_R$, the following expressions can be written for the anodic voltages at the receiver, for the target surface 1, $V_1$, and 2, $V_2$:

$$V_1 = \mathrm{R_L} \cdot \mathrm{R_S} \cdot \left(P_B \cdot \rho \cdot \frac{e^{-2 \cdot \gamma \cdot d_1}}{d_1^2}\right) \tag{19}$$

$$V_2 = \mathrm{R_L} \cdot \mathrm{R_S} \cdot \left(P_B \cdot \rho \cdot \frac{e^{-2 \cdot \gamma \cdot d_2}}{d_2^2}\right) \tag{20}$$

where:

$\mathrm{P_B}$ = parameter accounting for the laser emitter power, for the window efficiencies and for the geometric characteristics of the beam;

$\rho$ = target reflectivity.

This is the author pre-publication version. This paper does not include the changes arising from the revision, formatting and publishing process. The final paper that should be used for referencing is:

A. Gardi, R. Sabatini and S. Ramasamy, "Stand-off Measurement of Industrial Air Pollutant Emissions from Unmanned Aircraft." Proceedings of IEEE International Conference on Unmanned Aircraft Systems (ICUAS 2016). Arlington, VA (USA), June 2016. Print ISBN: 978-1-4673-9333-1

The derived relation between the two sensed voltages is therefore:

$$\frac{V_1}{V_2} = \frac{P_{O1}}{P_{O2}} \cdot \frac{d_2^2}{d_1^2} \cdot e^{2 \cdot \gamma (d_2 - d_1)} \quad (21)$$

where:

$P_{O1,\,2}$ = transmitted laser powers (W)

The ground-level extinction coefficient relative to both spectral lines is therefore calculated as:

$$\gamma = \frac{1}{2\,\Delta d} \ln \left[ \frac{\left(\frac{V_1}{P_{O1}}\right) d_1^2}{\left(\frac{V_2}{P_{O2}}\right) d_2^2} \right] \quad (22)$$

where $\Delta d = d_2 - d_1 \geq 1\ km$, as previously discussed.

The total uncertainty related to the extinction coefficient in eq. 10 is[18]:

$$\sigma_\gamma^2 = \frac{1}{(2\Delta \mathrm{d})^2} \cdot \left[ \left( \frac{\sigma_{V1}^2}{V_1^2} + \frac{\sigma_{V2}^2}{V_2^2} \right) + \left( \frac{\sigma_{P_{O1}}^2}{P_{O1}^2} + \frac{\sigma_{V_{O2}}^2}{P_{O2}^2} \right) \right] + \frac{\gamma^2}{\Delta \mathrm{d}^2} \left[ \left( \mathrm{d}_2 + \frac{1}{\gamma} \right)^2 \cdot \frac{\sigma_{\mathrm{d}2}^2}{\mathrm{d}_2} + \left( \mathrm{d}_1 + \frac{1}{\gamma} \right)^2 \cdot \frac{\sigma_{\mathrm{d}1}^2}{\mathrm{d}_1^2} \right] \quad (23)$$

By employing the same laser emitter for the ground and airborne systems we may assume constant errors in voltage and power, $\sigma_V / V$ and $\sigma_{Po} / P_O$. Considering also the distance $\Delta d$ several orders of magnitude higher than the extinction coefficient and rearranging the terms we obtain:

$$\sigma_\gamma = \frac{1}{\Delta\, \mathrm{d}} \sqrt{\frac{1}{2} \left( \frac{\sigma_V^2}{V^2} + \frac{\sigma_{P_O}^2}{P_O^2} \right)} \quad (24)$$

In the calibration system design, it must be ensured that the overall uncertainty is an order of magnitude lower than the one associated with the bistatic LIDAR measurement system. From eq. 11, neglecting the uncertainty in $\Delta\psi$, the error on the pollutant column density measurement $N_{CO_2}$ for the calibration system layout is:

$$\sigma_{CAL,N_{CO_2}} = \frac{1}{\Delta\psi} \cdot \sqrt{2[\sigma_\gamma^2 - cov(\gamma_{ON}, \gamma_{OFF})]} \quad (25)$$

By introducing the uncertainty in the extinction coefficient from (16), we finally obtain:

$$\sigma_{CAL,N_{CO_2}} = \frac{1}{\Delta\psi} \sqrt{\frac{1}{\Delta d} \left( \frac{\sigma_V^2}{V^2} + \frac{\sigma_{P_O}^2}{P_O^2} \right) - 2 \cdot cov(\gamma_{ON}, \gamma_{OFF})} \quad (26)$$

This result clearly supports the selection of large relative distances between the targets, ideally in the range of 1~3 km or more if available. Similar distances are comparable to the typical runway lengths at major airports. Therefore, the calibration system may ideally be collocated parallel and in proximity of a runway, outside of the Instrument Landing System (ILS) sensitive areas where applicable.

## X. LIDAR Error Estimation

The uncertainty associated with the measurement of the molecular volume concentration, derived from eq. 12, is:

$$\sigma_{\tilde{n}_P} = \frac{1}{D \cdot \Delta\psi} \sqrt{\begin{matrix} \left( \frac{\sigma_{R_{ON/OFF}}}{R_{ON/OFF}} \right)^2 + \\ + \left( \frac{\sigma_D \ln R_{ON/OFF}}{D} \right)^2 + \\ + \left( \frac{\sigma_{\Delta\psi} \ln R_{ON/OFF}}{\Delta\psi} \right)^2 \end{matrix}} \quad (27)$$

For a preliminary estimation, we introduced representative errors on the first two quadratic terms in eq. 17, specific to the bistatic DIAL implementation. Errors were introduced on the distance, $\sigma_D$ , and on the differential energy measurement, which is translated into $\sigma_{R_{ON/OFF}}$ by means of the Bidirectional Reflectance Distribution Function (BRDF) of the target surface [18]. Assuming the operational conditions summarised in Table 4 and injecting source errors detailed in Table 5, the resulting relative error for the $CO_2$ volume density was calculated as $\frac{\sigma_{\tilde{n}_P}}{\tilde{n}_P}$ = 6.77 % [15].

TABLE IV. Assumed worst-case operative conditions [15].

| Parameter | Value |
|---|---|
| Horizontal distance between the UA and the target surface | 1000 m |
| UA Height Above Ground Level (AGL) | 150 m |
| $CO_2$ volume density | 300 ppm |

TABLE V. Assumed source errors [15].

| Source | Magnitude | Affected Term | Error |
|---|---|---|---|
| Discrepancy in the incident angle between $E(\lambda_{ON})$ and $E(\lambda_{OFF})$ | 5° azimuth 5° elevation | $\frac{\sigma_{R_{ON/OFF}}}{R_{ON/OFF}}$ | 3.04 % |
| Degraded UA navigation performance | 20 m horizontally 15 m vertically | $\frac{\sigma_D}{D}$ | 2.47% |

These preliminary results associated with the very low error figures from the monostatic Integral Path Differential Absorption (IPDA) LIDAR experimental campaigns [24] and with the estimated performance of the in-situ calibration technique, contribute to supporting the validity of the proposed bistatic DIAL measurement technique for high accuracy sensing of aviation-related pollutant concentrations. Experimental testing will be required to further corroborate these preliminary findings.

## XI. Conclusions and Future Work

This paper focusses on the development of an innovative bistatic LIDAR system for the stand-off measurement of pollutant concentrations. The system is specifically conceived to monitor the molecular and aerosol pollutant emissions around industrial complexes and major transport hubs from stand-off locations.

This is the author pre-publication version. This paper does not include the changes arising from the revision, formatting and publishing process. The final paper that should be used for referencing is:

A. Gardi, R. Sabatini and S. Ramasamy, "Stand-off Measurement of Industrial Air Pollutant Emissions from Unmanned Aircraft." Proceedings of IEEE International Conference on Unmanned Aircraft Systems (ICUAS 2016). Arlington, VA (USA), June 2016. Print ISBN: 978-1-4673-9333-1

The theoretical model inversion relationships for molecular and aerosol measurements were presented. The Differential Absorption LIDAR (DIAL) measurement principle can be adopted for accurately measuring the concentrations of molecular species, neglecting parasite effects such as atmospheric visibility, particulate and precipitation, and contributing to the overall accuracy and reliability of the proposed technique. The uncertainty analysis for $CO_2$ column density measurements showed that the proposed technique produces satisfactory results even in degraded meteorological conditions, which are comparable to the more complex and relatively costly monostatic LIDAR techniques currently available. Current research activities are investigating the experimental test bench development and the full-scale implementation of the system also addressing nitrogen oxides ($NO_X$), sulphur oxides ($SO_X$), and Volatile Organic Compounds (VOC) taking advantage of the recent availability of tuneable laser emitters for multi-species detection. The research activities will involve laboratory testing as well as flight testing in various representative conditions. In particular, the development of the airborne component will benefit from the concurrent research activities on UA-based LIDAR systems [25-27]. The UA will be equipped with Differential GPS-based Time-and-Space-Position-Information (TSPI) systems that were developed for augmented navigation performance of both manned and unmanned aircraft [28, 29] in combination with integrity augmentation systems [30, 31]. The experimental flight testing activity will be performed in a suitably developed laser test range in full compliance with eye-safety requirements [18, 23, 32].

## XII. References

[1] M. Wendisch and J.-L. Brenguier (Eds.), *Airborne Measurements for Environmental Research - Methods and Instruments*, 1st ed. Wiley-VCH Verlag, Weinheim, Germany, 2013.

[2] E. V. Browell, S. Ismail, and W. B. Grant, "DIAL", in *Encyclopedia of Atmospheric Sciences*, 2003.

[3] D. E. Heard, "Field Measurements of Atmospheric Composition", in *Analytical Techniques for Atmospheric Measurement*, ch. 1, pp. 1-71, D. E. Heard, Ed., Blackwell Publishing, Oxford, UK, 2006.

[4] J. Pelon, G. Vali, G. Ancellet, G. Ehret, P. H. Flamant, S. Haimov, *et al.*, "LIDAR and RADAR Observations", in *Airborne Measurements for Environmental Research: Methods and Instruments*, pp. 457-526, Wiley-VCH, 2013.

[5] J. B. Abshire, A. Ramanathan, H. Riris, J. Mao, G. R. Allan, W. E. Hasselbrack, *et al.*, "Airborne measurements of CO2 column concentration and range using a pulsed direct-detection IPDA lidar", *Remote Sensing*, vol. 6, pp. 443-469, 2013. DOI: 10.3390/rs6010443

[6] R. Sabatini, M. A. Richardson, H. Jia, and D. Zammit-Mangion, "Airborne laser systems for atmospheric sounding in the near infrared", *SPIE 8433 Laser Sources and Applications, Photonics Europe 2012*, Brussels, Belgium, 2012. DOI: 10.1117/12.915718

[7] D. Wunch, G. C. Toon, P. O. Wennberg, S. C. Wofsy, B. B. Stephens, M. L. Fischer, *et al.*, "Calibration of the total carbon column observing network using aircraft profile data", *Atmospheric Measurement Techniques*, vol. 3, pp. 1351-1362, 2010. DOI: 10.5194/amt-3-1351-2010

[8] J. B. Abshire, H. Riris, G. R. Allan, C. J. Weaver, J. Mao, X. Sun, *et al.*, "Pulsed airborne lidar measurements of atmospheric CO2 column absorption", *Tellus, Series B: Chemical and Physical Meteorology*, vol. 62, pp. 770-783, 2010. DOI: 10.1111/j.1600-0889.2010.00502.x

[9] J. Mao, S. R. Kawa, J. B. Abshire, and H. Riris, "Sensitivity studies for space-based laser measurements of atmospheric CO2 concentration towards future NASA mission ascends", *30th IEEE International Geoscience and Remote Sensing Symposium (IGARSS 2010)*, Honolulu, HI, USA, 2010, pp. 643-645. DOI: 10.1109/IGARSS.2010.5651523

[10] M. A. Krainak, A. E. Andrews, G. R. Allan, J. F. Burris, H. Riris, X. Sun, *et al.*, "Measurements of atmospheric CO2 over a horizontal path using a tunable-diode-laser and erbium-fiber-amplifier at 1572 nm", *Conference on Lasers and Electro-Optics 2003 (CLEO '03)*, Baltimore, MD, USA, 2003, pp. 878 - 881

[11] H. Riris, J. B. Abshire, G. Allan, J. F. Burris, J. Chen, S. R. Kawa, *et al.*, "A laser sounder for measuring atmospheric trace gases from space", *SPIE 6750, Lidar Technologies, Techniques, and Measurements for Atmospheric Remote Sensing III*, Florence, Italy, 2007. DOI: 10.1117/12.737607

[12] A. Gardi, R. Sabatini, S. Ramasamy, and K. de Ridder, "4-Dimensional Trajectory Negotiation and Validation System for the Next Generation Air Traffic Management", *AIAA Guidance, Navigation, and Control Conference (GNC 2013)*, Boston, MA, USA, 2013. DOI: 10.2514/6.2013-4893

[13] A. Gardi, R. Sabatini, S. Ramasamy, and T. Kistan, "Real-Time Trajectory Optimisation Models for Next Generation Air Traffic Management Systems", *Applied Mechanics and Materials*, vol. 629, pp. 327-332, 2014. DOI: 10.4028/www.scientific.net/AMM.629.327

[14] A. Gardi, R. Sabatini, and G. Wild, "Unmanned aircraft bistatic lidar for CO2 colum density determination", *IEEE Metrology for Aerospace (MetroAeroSpace 2014)*, Benevento, Italy, 2014. DOI: 10.1109/MetroAeroSpace.2014.6865892

[15] A. Gardi, R. Sabatini, and S. Ramasamy, "Bistatic LIDAR System for the Characterisation of Aviation-Related Pollutant Column Densities", *Applied Mechanics and Materials*, vol. 629, pp. 257-262, 2014. DOI: 10.4028/www.scientific.net/AMM.629.257

[16] A. Gardi and R. Sabatini, "Bistatic DIAL for Multi-Species Aviation Pollutant Measurements from RPAS", *SAE Technical Paper 2015-01-2477*, 2015. DOI: 10.4271/2015-01-2477

[17] R. Sabatini and M. A. Richardson, "Innovative methods for planetary atmospheric sounding by lasers", *AIAA Space 2008 Conference*, San Diego, CA, USA, 2008. DOI: 10.2514/6.2008-7670

[18] R. Sabatini and M. A. Richardson, *Airborne Laser Systems Testing and Analysis*, RTO AGARDograph AG-300 Vol. 26, Flight Test Instrumentation Series, Systems Concepts and Integration Panel (SCI-126), NATO Science and Technology Organization, 2010.

[19] R. Sabatini and M. A. Richardson, "Novel atmospheric extinction measurement techniques for aerospace laser system applications", *Infrared Physics and Technology*, vol. 56, pp. 30-50, 2013. DOI: 10.1016/j.infrared.2012.10.002

[20] F. G. Gebhardt, "High Power Laser Propagation", *Applied Optics*, vol. 15, pp. 1479-1493, 1976

[21] D. Müller, F. Wagner, U. Wandinger, A. Ansmann, M. Wendisch, D. Althausen, *et al.*, "Microphysical particle parameters from extinction and backscatter lidar data by inversion with regularization: Experiment", *Applied Optics*, vol. 39, pp. 1879-1892, 2000

This is the author pre-publication version. This paper does not include the changes arising from the revision, formatting and publishing process. The final paper that should be used for referencing is:

A. Gardi, R. Sabatini and S. Ramasamy, "Stand-off Measurement of Industrial Air Pollutant Emissions from Unmanned Aircraft." Proceedings of IEEE International Conference on Unmanned Aircraft Systems (ICUAS 2016). Arlington, VA (USA), June 2016. Print ISBN: 978-1-4673-9333-1

[22] C. D. Rodgers, *Inverse methods for atmospheric sounding: Theory and practice* vol. 2, World scientific Singapore, 2000.

[23] R. Sabatini and M. A. Richardson, "A new approach to eye-safety analysis for airborne laser systems flight test and training operations", *Optics and Laser Technology*, vol. 35, pp. 191-198, 2003. DOI: 10.1016/S0030-3992(02)00171-8

[24] J. B. Abshire, H. Riris, C. J. Weaver, J. Mao, G. R. Allan, W. E. Hasselbrack, *et al.*, "Airborne measurements of CO2 column absorption and range using a pulsed direct-detection integrated path differential absorption lidar", *Applied Optics*, vol. 52, pp. 4446-4461, 2013. DOI: 10.1364/AO.52.004446

[25] R. Sabatini, A. Gardi, and M. A. Richardson, "LIDAR Obstacle Warning and Avoidance System for Unmanned Aircraft", *International Journal of Mechanical, Aerospace, Industrial and Mechatronics Engineering*, vol. 8, pp. 62-73, 2014

[26] R. Sabatini, A. Gardi, S. Ramasamy, and M. A. Richardson, "A Laser Obstacle Warning and Avoidance System for Manned and Unmanned Aircraft", *IEEE Metrology for Aerospace (MetroAeroSpace 2014)*, Benevento, Italy, 2014, pp. 616-621. DOI: 10.1109/MetroAeroSpace.2014.6865998

[27] R. Sabatini, A. Gardi, and S. Ramasamy, "A Laser Obstacle Warning and Avoidance System for Unmanned Aircraft Sense-and-Avoid", *Applied Mechanics and Materials*, vol. 629, pp. 355-360, 2014. DOI: 10.4028/www.scientific.net/AMM.629.355

[28] R. Sabatini, "High Precision DGPS and DGPS/INS Positioning for Flight Testing", in *RTO-MP-043 - 6th Saint Petersburg International Conference on Integrated Navigation Systems*, pp. 18-1 to 18-17, NATO Research and Technology Organization (RTO), Saint Petersburg, Russia, 1999.

[29] R. Sabatini and G. B. Palmerini, *Differential Global Positioning System (DGPS) for Flight Testing*, RTO AGARDograph AG-160 Vol. 21, Flight Test Instrumentation Series, Systems Concepts and Integration Panel (SCI-135), NATO Science and Technology Organization, 2008.

[30] R. Sabatini, T. Moore, and C. Hill, "A new avionics-based GNSS integrity augmentation system: Part 1 - Fundamentals", *Journal of Navigation*, vol. 66, pp. 363-384, 2013. DOI: 10.1017/S0373463313000027

[31] R. Sabatini, T. Moore, and C. Hill, "A new avionics-based GNSS integrity augmentation system: Part 2 - Integrity flags", *Journal of Navigation*, vol. 66, pp. 501-522, 2013. DOI: 10.1017/S0373463313000143

[32] R. Sabatini, "Innovative Flight Test Instrumentation and Techniques for Airborne Laser Systems Performance Analysis and Mission Effectiveness Evaluation", *IEEE Metrology for Aerospace (MetroAeroSpace 2014)*, Benevento, Italy, 2014, pp. 1-17. DOI: 10.1109/MetroAeroSpace.2014.6865886